Comparison of numerical analyses of a composite wing component subjected to 4-point bending

C. Bisagni [a,*], A. Raimondo [a], I. Atanasovska [b], M. Milic [c], R. Troian [d], G. Frulla [e], A. Polla [e], Ö.N. Cora [f], M.L. Bekci [f], B. Henriques [g], M.F.S.F. de Moura [g], F. Almudaihesh [h], S. Grigg [h]

[a] *Faculty of Aerospace Engineering, Delft University of Technology, Delft, the Netherland*
[b] *Mathematical Institute of the Serbian Academy of Sciences and Arts, Belgrade, Serbia*
[c] *Faculty of Mechanical Engineering, University of Belgrade, Belgrade, Serbia*
[d] *Institut National des Sciences Appliquées de Rouen, Laboratory of Mechanics, Rouen, France*
[e] *Politecnico di Torino, DIMEAS, Torino, Italy*
[f] *Department of Mechanical Engineering, Karadeniz Technical University, Trabzon, Turkey*
[g] *Department of Mechanical Engineering, University of Porto, Porto, Portugal*
[h] *School of Engineering, Cardiff University, Cardiff, UK*

ARTICLE INFO

ABSTRACT

In this paper, a comparison between six finite element models of a representative wing structural component performed in the context of Optimised Design for Inspection (ODIN) project of the European Cooperation in Science and Technology (COST) is presented. Six partners from six different countries involved in the project received the drawing of the structure, the material properties, the loading and boundary conditions. Each partner, based on their background and experience in numerical analyses, developed a finite element model with different levels of details and accuracy and performed a blind prediction of the structural behaviour of the wing component. The numerical results are presented and compared with the experimental test data conducted at Cardiff University.

1. Introduction

Over the past decades, the advancements in analytical and computational methods, such as the Finite Element (FE) method, have led to developing of increasingly accurate models for the structural analysis. The exponential growth of computational capabilities supported by advanced algorithms have provided researchers with several software packages and numerical techniques to accurately predict the behaviour of complex structures with reasonable computational times. Despite the availability of such a variety of numerical tools and techniques, the blind prediction of the structural response of aeronautical structures in composite materials still represents a significant challenge. Several round-robin and benchmark exercises have been organised over the years to evaluate the state-of-the-art in this area.

For example, the Polymers and Composites Task Group of the European Group on Fracture organised three round-robin exercises to determine mode I and mode II interlaminar fracture toughness of glass and carbon fibre-reinforced thermoset and thermoplastic composites

[1–3]. Soden and Hilton organised an exercise aimed to compare the predicting capabilities of the failure theories for available glass and carbon fibre-reinforced thermoset composites directly with each other and against experimental data [4,5]. More recently, the US Air Force Research Laboratory performed benchmark exercises for composite progressive damage analysis methods using unnotched and open-hole composite coupons under both static and fatigue loading [6,7].

Most of the works found in the literature relates to comparative studies on coupons or small specimens, while there is a lack of research dealing with larger and more complex structures. This study presents a preliminary comparison of different FE modelling techniques to predict the structural response of a relatively complex representative wing structure made of metals and composite materials.

Only a few studies can be found in literature regarding numerical analysis of composite wing structures, and they present different levels of detail. Parametric finite element models of wing structures have been performed, considering the design and optimisation with strength and buckling constraints [8] or stiffness and aeroelastic constraints [9,10]. A
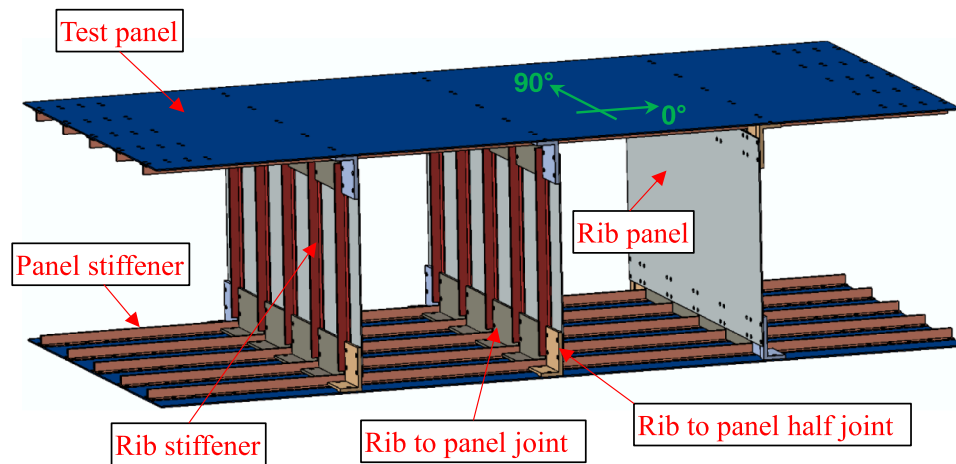
Fig. 1. Representative wing component.

model based on the equivalent strength and stiffness method is developed in [11] to reduce the computational time in the preliminary design phase. A global-local approach is used in [12] together with progressive failure methodologies to predict the structural performance of bonded repairs under static and fatigue loads. A full three-dimensional model based on shell elements is presented in [13] to investigate the buckling response of composite-aluminium wing structure, while in [14] a three-dimensional finite element model based on solid elements is conducted to evaluate the local response of the bolted joints of a composite-aluminium wing structure.

The aim of this study is to compare different modelling assumptions in terms of element type adopted for the discretisation, boundary conditions, connection between components, type of numerical solver algorithm and to investigate their effect on the structural response of a representative wing structures subjected to 4-point bending load. A preliminary experimental test is also performed and the data of the test are used to compare and validate the different numerical models.

The work presented here is part of the Optimised Design for Inspection (ODIN) project [15] of the European Cooperation in Science and Technology (COST) [16]. COST is a European funded organisation for research and innovation networks with the primary goal of helping connect research initiatives across Europe and beyond, and enabling researchers and innovators to grow their ideas in any science or technology field by sharing them with their peers. The ODIN project seeks to develop optimised structures by integrating ultrasonic wave-based non-destructive evaluation, energy harvesting and wireless sensor technologies in the design conception phase. Working Group 1 in the ODIN project aims to establish design and analysis criteria for a representative wing structure. This knowledge will be shared with other working groups to realise the overall goal of ODIN.

Upon a few iterations with Cardiff University, which manufactured and tested the structure, the partners of ODIN reached a design of the wing component. The structure comprises of two flat composite panels with ribs and stiffeners made of aluminium alloys, tested under 4-point bending. Then, each partner received the structure CAD model, the materials properties of the different components, the boundary and the selected loading conditions.

Six partners of ODIN, with backgrounds in numerical analyses, developed their finite element models with different levels of details and accuracy and performed a blind prediction of the structural behaviour of the representative wing structure.

The research group from the Faculty of Aerospace Engineering of Delft University of Technology involved in the project ODIN, here shortened as TU DELFT, is experienced in the development of numerical methodologies for the analysis of damage propagation in composite materials at the coupon and structural levels under quasi-static and

fatigue loading conditions [17,18].

The members of the Mechanical Department of the University of Porto involved in ODIN, here named FEUP, have experience regarding progressive damage analysis in composites and composite bonded joints. They developed cohesive zone models suitable for quasi-static fracture characterisation under mixed-mode I+II loading and fatigue/fracture under mixed-mode I+II loading [19,20]. These models are particularly useful when designing structural components concerning damage identification and its progression under quasi-static and fatigue loading.

The Karadeniz Technical University group involved in ODIN, here shortened as KTU, has a considerable background in FE analysis and adopted it in various fields, including metal forming and modelling of the powder compaction process [21,22].

The research team BELGRADE consists of researchers from the University of Belgrade and from the Mathematical Institute of the Serbian Academy of Sciences and Arts in Belgrade. They have significant research experience in FE analysis, considering modelling of different complex structures with a special emphasis on nonlinear contact analysis [23], and structural beam-shell analysis [24] and composite structures in aerospace engineering.

The structural research group in Politecnico di Torino involved in ODIN, here shortened as POLITO, has experience in implicit and explicit numerical modelling techniques for the analysis of the damage in composite structures. POLITO has studied stiffened panels using a numerical procedure and with selected experimental activity [25]. Recently, new LS-DYNA simulations have been performed in static composite structural components and investigating impact induced damage effect and propagation [26].

The working group from Institut National des Sciences Appliquées de Rouen involved in ODIN, here named INSA, specialises in robust topology and shape optimisation for various applications. The numerical models they develop satisfy the compromise between the computational time-cost and plausible mechanical behaviour of the structure [27,28].

This paper aims to compare the numerical predictions obtained by the six partners using various commercially available FE codes and different modelling strategies. Section 2 of this paper describes the wing structure and the loading fixture, together with the list of the different components and material properties. Section 3 reports the FE models of each partner, while Section 4 describes the setup of the tests. The analyses results obtained by each partner are presented and compared to the experimental data in Section 5.

2. Wing component

The representative wing component analysed in this work comprises two test panels on the top and bottom, consisting of flat composite
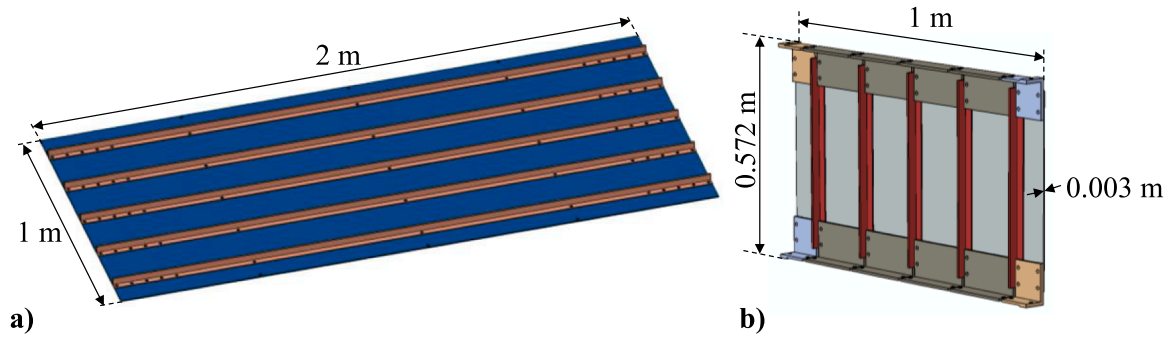
Fig. 2. Main parts of wing component: (a) Test panel; (b) Rib panel.

Table 1
Wing components and their materials.

Designation	Quantity	Material
Test panel	2	18 plies of USN150B $[-45/0/45/0/90/0/-45/0/45]_s$
Panel stiffener (T-shape stiffener)	10	Al 6063AT6
Rib panel	3	Al 6082AT6
Rib stiffener (T-shape stiffener)	15	Al 6063AT6
Rib to panel joint	24	Al 6082AT6
Rib to panel half joint	12	Al 6082AT6

Table 2
Material properties of aluminium alloys.

Material	σ_y[MPa]	E[MPa]	ν	ρ[g/cm^3]
Al 6063AT6	170	70,000	0.33	2.7
Al 6082AT6	260			

Table 3
USN150B composite ply properties.

E_{11} [MPa]	131,000	X_t [MPa]	2000
$E_{22} = E_{33}$ [MPa]	8000	$Y_t = Z_t$ [MPa]	61
$G_{12} = G_{13}$ [MPa]	4500	X_C [MPa]	2000
G_{23} [MPa]	3500	$Y_C = Z_C$ [MPa]	200
$\nu_{12} = \nu_{13}$	0.29	$S_{12} = S_{13}$ [MPa]	70
ν_{23}	0.47	S_{23} [MPa]	40
ρ [g/cm^3]	1.544	t_{ply} [mm]	0.194

panels stiffened with aluminium alloy T-shaped stiffeners and three ribs panels reinforced with aluminium alloy T-shaped stiffeners. All the components are connected using bolts through attachment plates, while the aluminium stiffeners are bonded to the composite panels with a two-component epoxy adhesive Araldite 420 A/B. Fig. 1 shows the wing component, while Fig. 2 shows a test panel and a rib panel and their dimensions.

The composite test panels are made of USN150B carbon/epoxy with stacking sequence $[-45/0/45/0/90/0/-45/0/45]_s$ and a total thickness of 3.5 mm. The remaining parts of the structure are made of two different aluminium alloys, 6063AT6 and 6082AT6. In Table 1, each component is listed together with the materials.

The material properties used in the numerical analyses for the aluminium alloys and the composite materials are reported in Table 2 and Table 3, respectively.

A rig is attached to each side of the wing component using four metal plates to introduce the loads and impose the boundary conditions. Half of the loading rig components and their dimensions are illustrated in Fig. 3.

The rigs and the attachment plates are made of two different types of steel. In Table 4, the fixture components are listed together with the

Table 4
Loading rig components and their materials.

Designation	Quantity	Material
Attachment plate (long)	2	Steel BS EN10025 S275JR
Attachment plate (short)	2	Steel BS EN10025 S275JR
Rig	2	Steel EN10219 S235JRH

Table 5
Material properties of steels rigs and attachment plates.

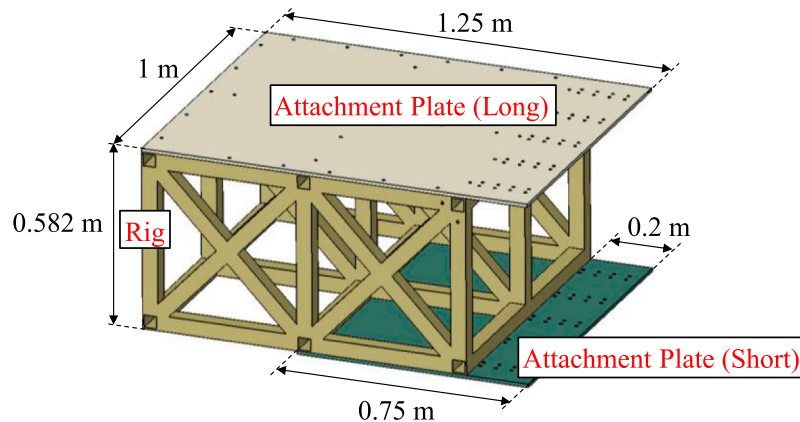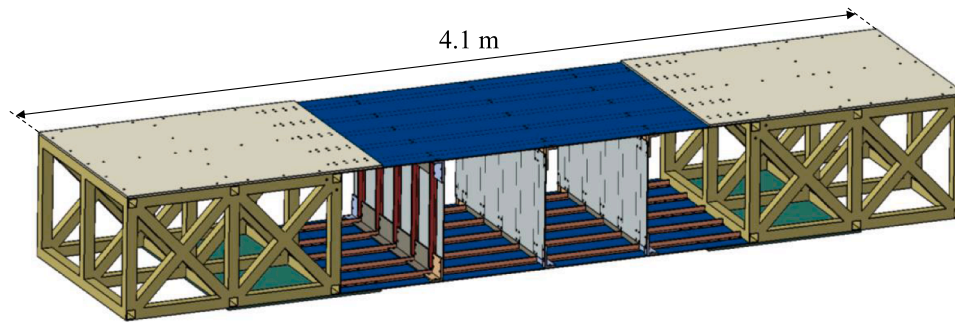| Material	σ_y[MPa]	E[MPa]	ν	ρ[g/cm^3]
Steel EN10219 S235JRH	235	210,000	0.3	7.5
Steel BS EN10025 S275JR	275			

Fig. 3. Half of the loading rig.

Fig. 4. Wing component with the loading rig.

Fig. 5. 4-point bending configuration.

Table 6
List of partners and FE models.

Partner	FE Code
Delft University of Technology (TU DELFT)	ABAQUS 2019 [29]
University of Porto (FEUP)	ABAQUS 6.11 [30]
Karadeniz Technical University (KTU)	ANSYS 2020 R2 [31]
Mathematical Institute of the Serbian Academy of Sciences and Arts and University of Belgrade (BELGRADE)	ANSYS Mechanical APDL 2019 R3 [32]
Politecnico di Torino (POLITO)	LS DYNA R11.1 [33]
Institut National des Sciences Appliquées de Rouen (INSA)	LS DYNA R9.1.0 [34]

material, while the material properties used in the numerical analyses are shown in Table 5.

The entire structure, which is of interest in the current study, comprises the wing component and the loading rig fixture and is shown in Fig. 4.

The wing structure is loaded in a 4-point bending configuration. Both loading points and supports featured a rectangular block attached to a circular beam to allow balance while the load is applied. The support span is 2 m apart, as shown in Fig. 5.

3. Finite element models

As part of the Working Group 1 activities of the COST in ODIN, six partners numerically analysed the representative wing component using different FE codes and independently established FE models. Each partner received the CAD model of the structure with the loading fixture and the material properties of the components, as reported in the previous section. The aim was to make a blind prediction of the structural behaviour of the wing component.

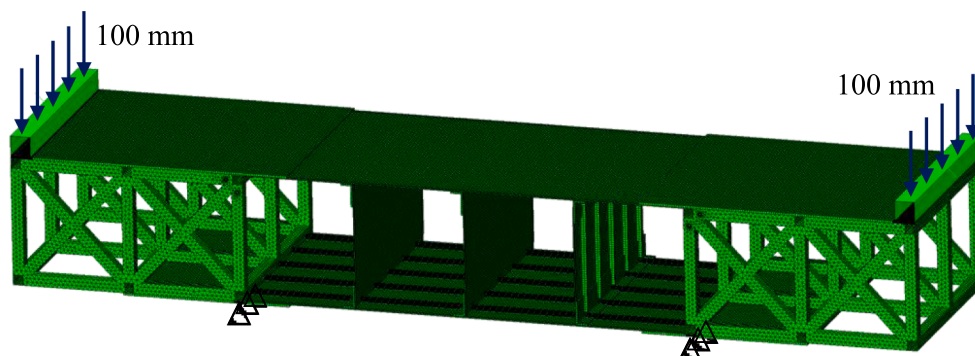The list of partners and the FE codes adopted is provided in Table 6.
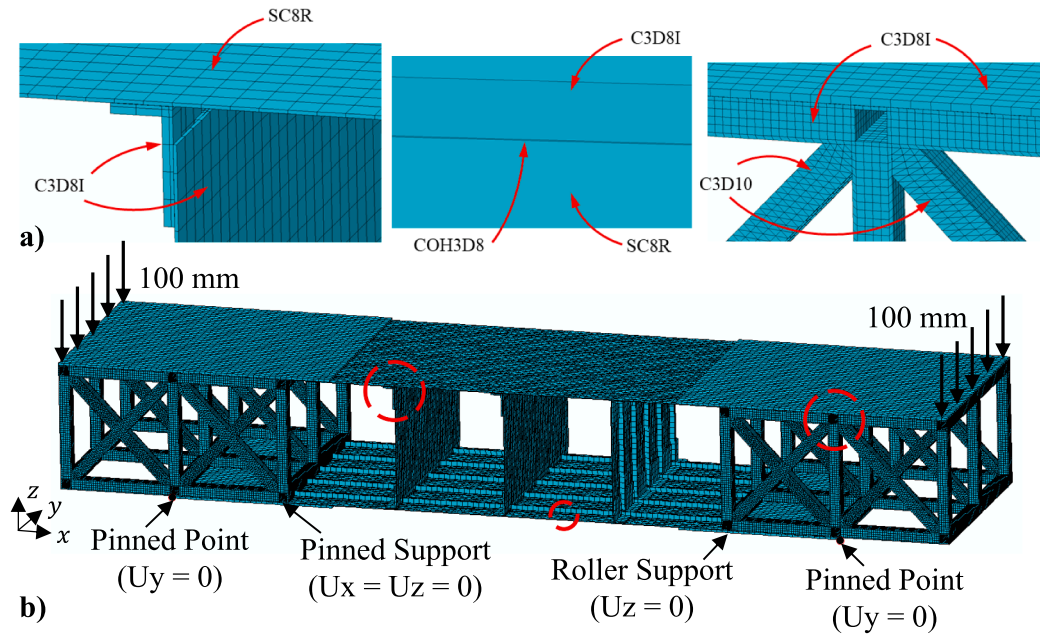

Fig. 6. FE model of TU DELFT.

Fig. 7. FE model of FEUP: (a) mesh details; (b) wing structure.

The following sections present a description of the FE models and the analysis strategy of each partner.

3.1. Finite element model of TU DELFT

The wing structural component is analysed using the FE code ABA-QUS 2019.

In the tested structure, bolts connect the components. However, in the FE model, the holes are neglected, and the components are connected using tie constraints. The structure is connected to the rigs using tie constraints between the attachment plates and the composite panels. The model is discretised using a combination of solid elements, C3D8R for the metal components, C3D10 for the rigs, and continuum shell elements SC8R with an average element size of 10 mm for the two composite panels. The total number of elements is around 300,000.

The load is introduced by modelling the two rectangular loading blocks with rigid surfaces, and boundary conditions are simulated by constraining the vertical displacement of the nodes on the bottom part of the structure in correspondence with the supports. The loading blocks are modelled as separate structures and surface-to-surface contacts with

hard contact and frictionless options are employed to simulate the contact between the loading blocks and the structure and avoid inter-penetration between the components. The FE model with boundary conditions is shown in Fig. 6.

The representative wing structure is analysed with the dynamic implicit solver under displacement-controlled conditions. A total displacement of 100 mm is applied to the two loading blocks. Hashin's failure criteria are adopted to detect any fibre/matrix damages within the composite laminates, but without considering the degradation of material properties after damage initiation.

3.2. Finite element model of FEUP

The wing structural component is analysed using the FE code ABA-QUS 6.11. No holes or bolts are considered to simplify the mesh and the analysis, and the connection between the parts is established using tie constraints.

The model is discretised using 8-node hexahedral solid elements with incompatible modes (C3D8I) for the stiffeners, the rib panels, the rib to panel joints and the attachment plates, while 8-node continuum shell
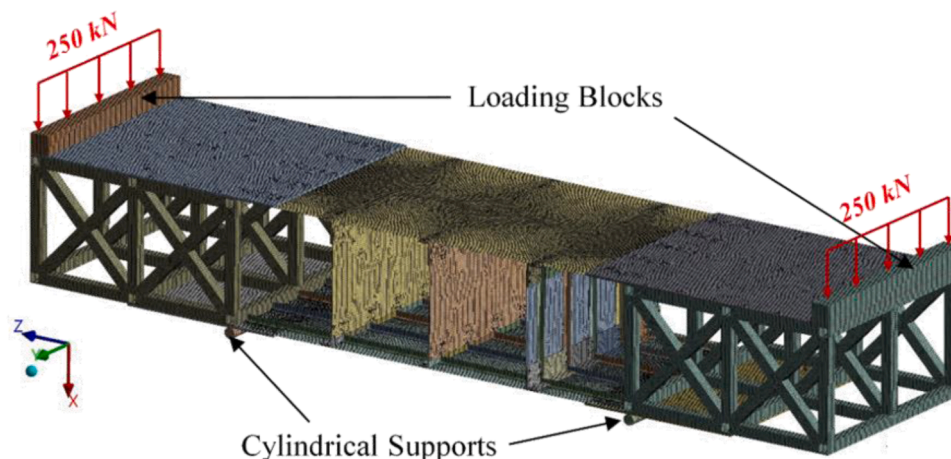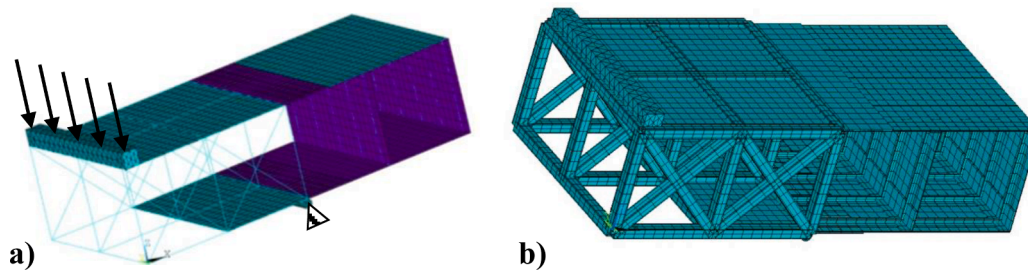

Fig. 8. FE model of KTU.

Fig. 9. FE model of BELGRADE:
a) Beam-shell-solid FE model; b) FE model with shape representation of beam-shell elements.

elements (SC8R) are employed for the composite panels. The test rig, is discretised using C3D8I and 10-node tetrahedral continuum solid elements (C3D10) due to the complexity of the geometry. The element types used in the model are shown in Fig. 7a. The Araldite 420 A/B is accounted for by adding a 0.05 mm layer of cohesive elements (COH3D8) with traction-separation behaviour in the interface between the stiffeners and the panels. Only the initial elastic stage is considered with a penalty stiffness per unit area of $K = 10^6$ N/mm^3. The nodes of one support are constraint along the x-direction to prevent rigid body motion of the structure. The single point constraints are adopted only on the nodes on the edge.

Different types of damage are considered: the yielding of the aluminium stiffeners with a von Mises yield criterion, the cohesive failure of the adhesive connection between the stiffeners and panels, and the composite fibre/matrix failure using Hashin's criteria. The boundary conditions adopted are shown in Fig. 7b. The structure is sustained on one pinned support and one roller support along its width; two points along the *x*-direction are fixed to avoid a rigid body motion in the *y*-direction. A total displacement of 100 mm is applied at the top of both extremities of the structure. Geometrical nonlinearities are considered, and the nonlinear equilibrium equations are solved using the Newton-Raphson method.

3.3. Finite element model of KTU

The finite element analysis of the representative wing component is performed using the commercial FE package ANSYS Workbench 20 R2. The numerical analysis has been performed before knowing the results of the experimental test, so a value of 500 kN has been chosen. The 500 kN loading is distributed uniformly through two rigid rectangular blocks on top of the structure along its width. The FE model established is illustrated in Fig. 8.

The blocks may only move vertically, while the cylindrical supports are constrained in all directions. The contacting nodes of the representative wing structure, however, are allowed to translate along X and Z axis, and free to rotate around the Y axis. Composite plates at the top and the bottom are discretised with shell elements, while solid elements are used for other components. The coefficient of friction is defined as 0.16 for the contacting surfaces of loading blocks with attachment plates (long) and supports with attachment plates (short). Other components are tied to each other either from nodes or contacting faces. Even though there are 478 pieces of M10 bolts at different lengths in the representative wing structure, they are not included in the model to save computational time. The total number of elements used in the model is about 560,000 with an average element size of 10 mm. Equivalent stress (von Mises) values were considered to check the possible failure of the components. Also, the maximum stress failure criterion was used to evaluate the possible failure of the top and bottom composite skins.

3.4. Finite element model of BELGRADE

The commercial FE software ANSYS Mechanical APDL 2019 R3 is used to analyse the wing component by static nonlinear analysis. Based on the full symmetry in the design, loading and constraints, the FE analysis is performed for only half of the structure with symmetry boundary conditions. The FE model is realised with a combination of shell, beam and solid elements. The wing component and the test rig are discretised with 3D 4-nodes shell elements (SHELL 181) and 2-nodes beam elements (BEAM 188), respectively while the two skin panels are modelled with 18-layers shell elements. The rectangular loading blocks and the circular supports are simulated as solid deformable steel bodies modelled with 8-nodes 3D brick solid elements (SOLID 185). The complete model comprises of 3315 finite elements with an average element size of about 50 mm. The connections between the elements of the main sub-structures (test specimen and test rig) which are realized in the real structures by fixed joints (rivets) and welded joints are tied to each other from nodes in order to save computational time. The contact between the rectangular loading block and the upper plate of the test rig is simulated by symmetric deformable contact pairs modelled with node-to-surface contact elements (CONTA 175) and 3D 4-nodes target finite elements (TARGE 170) with "always bonded" option, while the contact between the circular support and the test structure is modelled by the same types of contact-target finite elements and symmetric deformable characteristics of contact pairs with "initially bonded" option.

The boundary conditions are simulated by constraints: the displacement along the transverse direction is considered on a symmetry plane, while the circular support is fixed along the central axis. The rectangular loading block is constrained only by contact with the top plate of the test rig. The static loading conditions are defined on the loading block by applying half of the total external load in the range (0–500 kN) divided into 18 concentrated forces along the middle line of the top surface of the rectangular loading block. The loading and boundary conditions are schematically shown in Fig. 9a for a clearer presentation, while Fig. 9b shows the FE model with the thickness and size representations.

3.5. Finite element model of POLITO

The representative wing structure is analysed using the general-purpose dynamic finite element code LS-DYNA. The specific solver adopted is LS-DYNA R11.1 Single-Precision MPP architecture. An explicit non-linear quasi-static analysis is performed, and the model is fully discretised using shell elements with a combination of plates and boxes. Every component is represented by its mid-surface, and a specific z-offset is applied, taking the thickness into account. Standard shell elements are defined with ELFORM 16 (Fully-Integrated) and four Integration Points (NIP) through the thickness. The average mesh size selected for the entire model is 5 mm. The total amount of 2D shell elements for the entire structure is 880,364. In particular, 160,000 2D shell elements are adopted to define the two composite plates. Every composite element has several through-thickness integration points equal to the number of composite plies. The model has approximately 554 structural bolts which are modelled with Rigid Body Elements
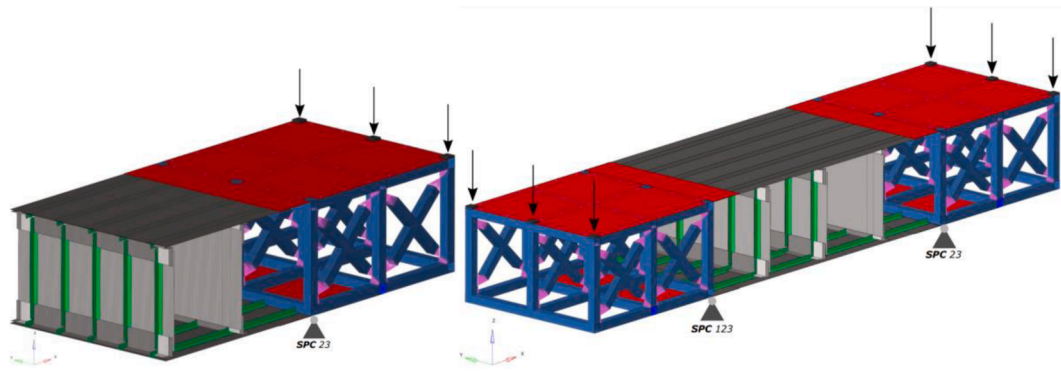
Fig. 10. FE model of POLITO.

(RBE). The contact behaviour between two adjacent components is simulated with the definition of a penalty-based surface-to-surface contact. The presence of a contact algorithm allows for avoiding penetrations and setting the correct contact stiffness between nearest FE elements. A Coulomb static friction coefficient of 0.16 is added inside the contact card. Elastic material (*MAT_001/*MAT_ELASTIC) is selected to characterise the mechanical behaviour of steel, aluminium and adhesive, while the composite behaviour is described with continuum damage model *MAT_058/* MAT_LAMINATED_COMPOSITE_FABRIC with Hashin failure criteria appropriate for UD layered composites. Solid Adhesive layers between the shell composite panels and aluminium stiffeners have been introduced into the model. A fully elastic behaviour has been considered in this preliminary investigation. The loading configuration applied to the structure is the same as reported in Fig. 5. The rigid loading block has been reproduced by the application of three equivalent forces for each side in the correspondence of the three vertical squared-box steel support structure as detailed in Fig. 10. Ideal lower supports are applied to the structure using the definition of Single Point Constraint (SPC). The structural hinge at the bottom-left of the structure is modelled with a through-width definition of SPC with 123 constrained DOF (XYZ-Displacement; Rotations not constrained). The right support is represented by SPC with only 23 DOF blocked (YZ-Displacement; Rotations not constrained). No vertical deflections of the supporting configuration under load are considered. The load is applied to the structure through a force controlling system. LS-DYNA characteristic composite failure criteria are adopted to describe the composite panel behaviour and conventional von Mises stress is selected to evaluate stress concentration in metallic isotropic materials. Fig. 10 shows the FE model. Numerical displacement evaluated at the position of expected lateral buckling deflection indicates the characteristic lateral bifurcation of the composite compressed panel. Moreover, the back-to-back numerical x-strain (Fig. 10) in the same position, shows the characteristic strain-reversal around 200 kN as a consequence of buckling situation. Thus, the critical load has been identified around 200–250 kN, and two post-critical buckles (anti-symmetrical) are determined.

3.6. Finite element model of INSA

The representative wing component is modelled in LS-DYNA using a simplified model to reduce the computational cost, eliminate numerical errors due to contact formulation and use the numerical model for a robust optimisation procedure. The geometry of the representative wing structure, the test rig and the loading conditions simplify the model as a beam loaded in 4-point bending. The analysis only focuses on the central part of the structure with a constant bending moment, and conditions of traction on the upper panel and compression on the lower panel are applied. The stiffeners elements are not directly modelled in order to simplify the geometry and use the model for future shape optimisation. Referring to Fig. 11, the grey colour corresponds to the steel plate, brown to the aluminium beams and blue to the composite panels. A traction force is applied in the x-direction on point A, while a compression force is applied on point B. Two symmetry planes allow for the modelling of only one-quarter of the structure. Symmetry planes are presented in Fig. 11a for the 2D projection and Fig. 11b for the 3D model. As boundary conditions, translations in the y-direction are blocked. For LS-DYNA implementation, the aluminium material is implemented using *MAT_001 card and the composite material using *MAT_022 card.

3.7. Comparison of finite element models

As reported in previous sections, the six partners adopted different FE codes and modelling strategies to analyse the wing component according to their backgrounds. Different levels of detail have been adopted in the modelling. Some partners preferred detailed modelling of each component, increasing the accuracy of the analysis but sacrificing the computational time, while others preferred simplifying assumptions to reduce the computational cost. Table 7 summarises the fundamental characteristics of the six FE models.
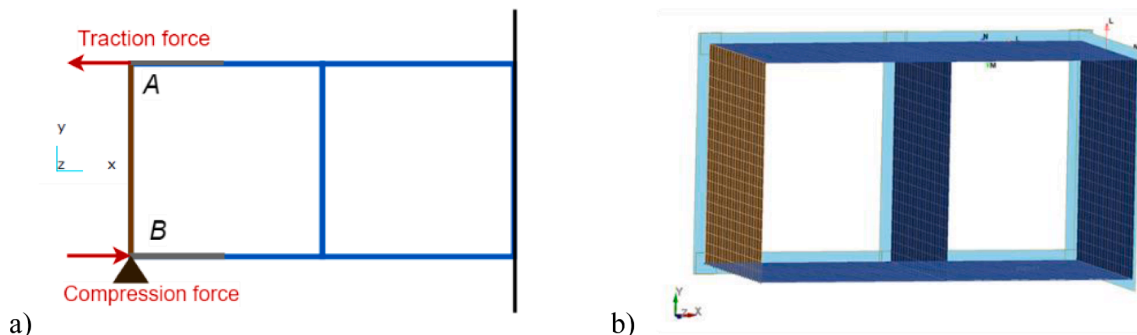

Fig. 11. FE model of INSA: (a) 2D model; (b) 3D model.

Table 7
Comparison between the six FE models.

Partner	Type of Analysis	Load/ Displacement controlled	Type of Elements	Number of Elements	Symmetry Conditions
TU DELFT	Dynamic Implicit	Displacement	Shell/ Solid	300,000	No
FEUP	Static Implicit	Displacement	Shell/ Solid	180,000	No
KTU	Static Implicit	Load	Shell/ Solid	560,000	No
BELGRADE	Static Implicit	Load	Shell/ Beam	4000	Yes
POLITO	Quasi-static Explicit	Load	Shell/ Beam	880,364	No
INSA	Quasi-static Implicit	Load	Shell	2400	Yes

4. Experimental set-up

The representative wing structure was manufactured at Cardiff University. Until now, a preliminary test was only performed, using the 4-point bending configuration shown in Fig. 12. The purpose of the experimental test shown in this work was to perform a preliminary set-up of the test apparatus and instrumentation in order to obtain data for a first validation of the numerical models, while the full test has not been yet performed and will be carried out in the near future.

Both the loading points and supports featured a rectangular block attached to a circular beam to allow balance while the load is applied.
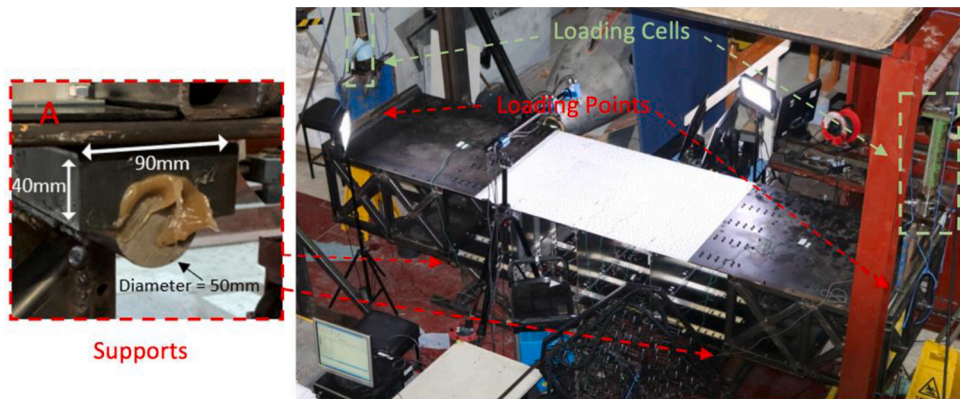
Load cells are attached to each loading jack with 50 tons of load capacity each, and the load is applied manually.

Following the recommendations of the partners involved in the project, the structure was equipped with Linear Variable Differential Transformers (LVDTs) to record the displacements and strain gauges to measure the deformation. The locations of LVDTs and strain gauges have not been reported since the strain gauges were not actually used during this preliminary test and the LVDTs were mounted on truss structures which increased the total compliance of the tested structure making their data unusable for numerical comparisons.

A total load of about 300 kN was applied equally on the loading points. The only failure observed up to this load was the debonding of four stiffeners, as highlighted in Fig. 13. The numbers represent the failure sequence of the stiffeners. Stiffener 1 and 2 were the first to debond around 250 kN, followed by stiffener 3 around 275 kN and stiffener 4 around 300 kN. At this stage, the load was stopped to avoid catastrophic failure, which could have led to damage to the instrumentation and the rig fixture.

5. Results and comparisons

The numerical results obtained from the analyses performed by the different partners and the experimental curve are reported in Fig. 14 in terms of load vs vertical displacement of the loading blocks.

Table 8 summarises the maximum load and displacement achieved by the numerical analyses, together with the experimental values.

The approaches to model the boundary conditions, the different levels of discretisation and the predicted behaviour of the structure in terms of load vs displacement are quite different amongst the partners
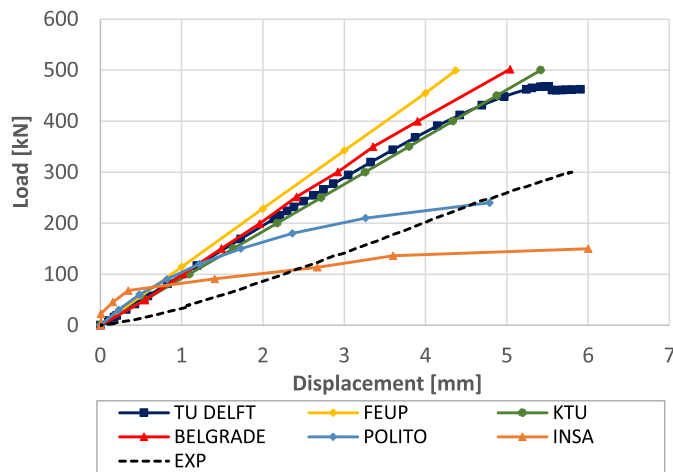

Fig. 12. Experimental setup at Cardiff University.

Fig. 13. Location of debonded stiffeners.

Fig. 14. Comparison of load-displacement curves.

Table 8
Numerical and experimental maximum loads and displacements.

Partner	Maximum Load [kN]	Maximum Displacement [mm]
TU DELFT	467	10
FEUP	499	4.4
KTU	500	5.4
BELGRADE	501	5
POLITO	300	16.5
INSA	181	9.7
EXP	300	5.8

because of the different modelling strategies, although there are some similarities.

It is possible to observe in Fig. 14 that all the numerical models exhibit almost the same initial stiffness. It can also be observed that the results can be grouped into two. Up to around 500 kN, the models by TU DELFT, FEUP, KTU and BELGRADE exhibit linear load-displacement behaviour, while the models by POLITO and INSA show a nonlinear response from the start of the loading. The numerical model developed

by INSA shows lower stiffness and buckling load since the connection elements are not directly modelled in order to simplify the geometry for future shape optimisation. In the POLITO analysis, the initial stiffness matches that of the other partners, while at higher loads the simulation follows the non-linear lateral deflection induced by critical and post-critical regime exhibiting a two-half-waves shape for the compressed panel on the bottom of the representative wing structure. When the FE models are compared with the experimental data, the actual structure has less stiffness and an almost linear load-displacement behaviour until 300 kN when the loading stops.

Fig. 15 reports the displacements obtained by the different numerical analyses at the LVDT5 and LVDT11 locations in the load function. LVDT5 and LVDT11 locations are at the bottom of the structure in correspondence with the loading blocks, as graphically illustrated in Fig. 16. Also in Fig. 15 it is possible to note that vertical deflection is linear for the most of the simulations while for POLITO result the LVDT behaviour is consistent to previous indicated pre-critical and post-critical behaviour for the compressed panel. The results of the numerical model developed by INSA are not reported since the test rig is not modelled in their model, and no data are available for these LVDT locations. The numerical curves are not compared to the experimental data, as the location of the LVDTs was changed before the test, positioning them on a supporting structure.

Figs. 17 and 18 show the deformed shapes with the vertical displacement contour plot of the analyses, as performed by the different partners at an applied load of 150 kN and 300 kN. As the numerical analyses carried out by the different partners reach different values of the maximum load, as shown in Table 8, these two load levels have been selected since they correspond to 50% and 100% of the maximum load achieved during the experimental test.

By observing the deformed shapes of the structure, it can be noted that during the initial linear behaviour, the structure rises in the central part while it lowers at both ends where the load is applied. As the applied load and displacement increase, the compressive load acting on the composite panel in the lower part of the representative wing structure causes the buckling of the entire composite skin and the T-shaped aluminium stringers. The post-buckling shapes obtained from the numerical models are consistent amongst the different partners with one sinusoidal wave in the longitudinal direction and no wave in the
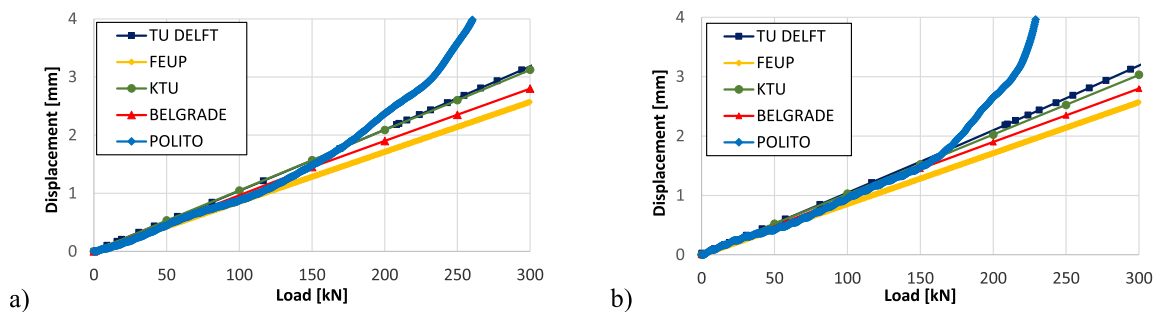

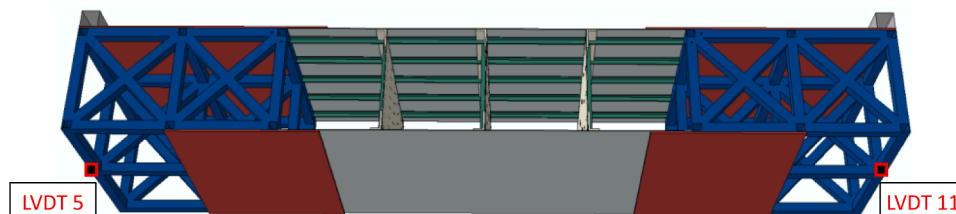**Fig. 15.** Comparison of load vs displacement measured from: (a) LVDT5; (b) LVDT11.
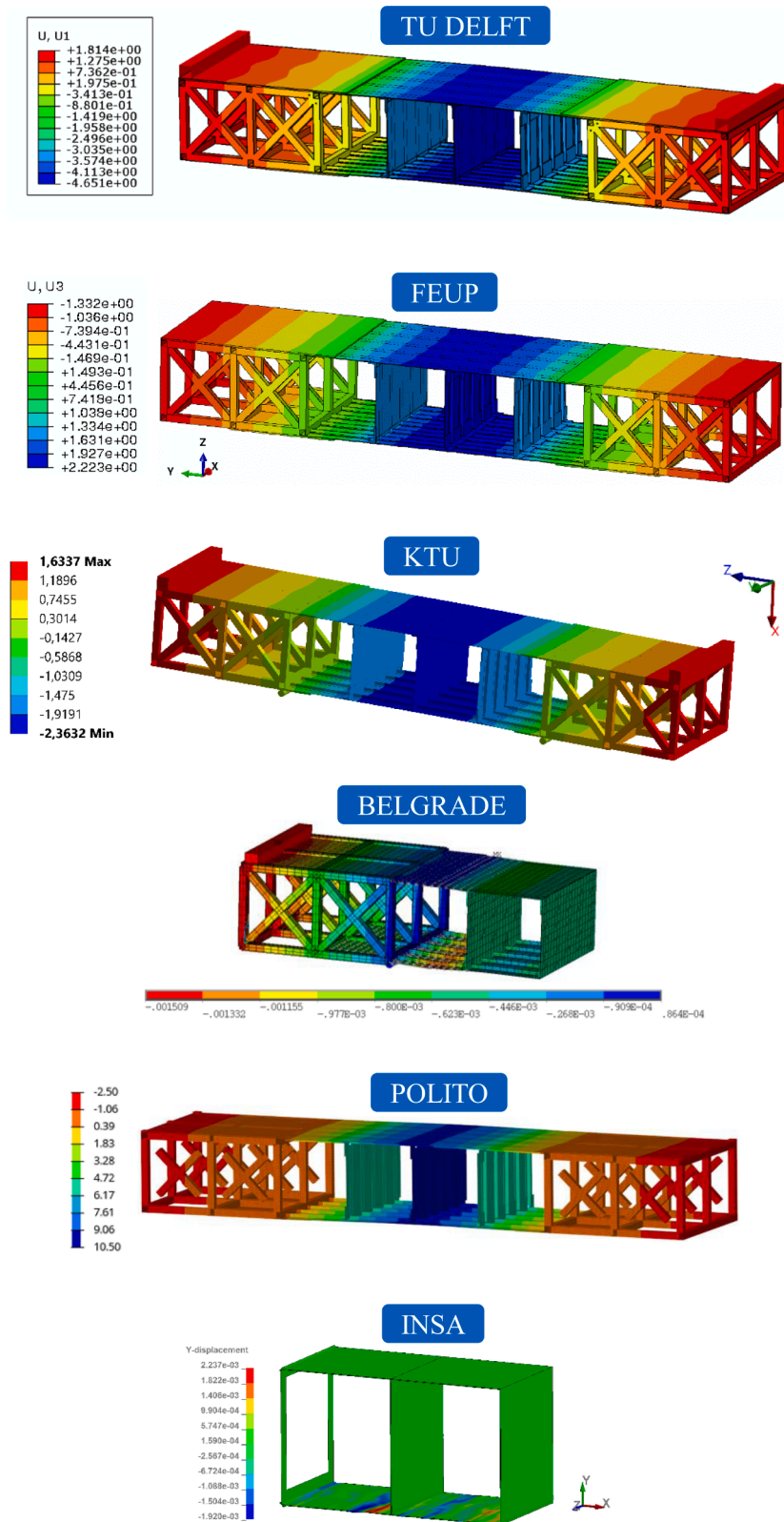

Fig. 16. Location of LVDTs.

Fig. 17. Deformed shapes of the wing structure at 150 kN.

transverse direction. The same instability phenomenon was observed during the experimental test. Fig. 19 reports images of the representative wing structure taken at the beginning of the test and after reaching the maximum load of 300 kN. The lower skin panel buckles at the maximum load, and the composite skin separates from the stringers due to the high out-of-plane stresses.

A combination of multiple factors can explain the differences in the numerical results regarding the measured data.

One of the main reasons is the material property. The material properties adopted in the numerical models have been obtained from
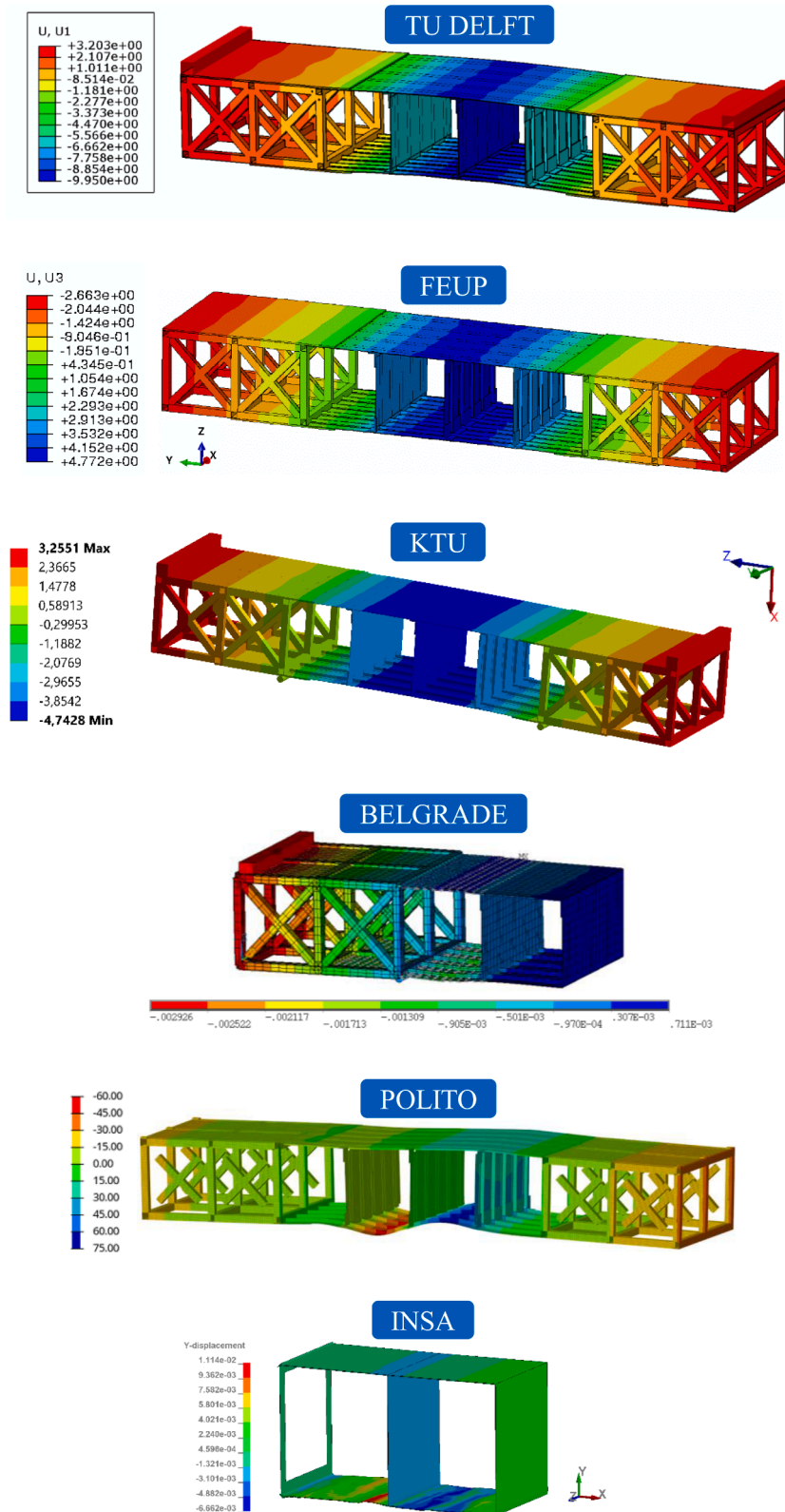
Fig. 18. Deformed shapes of the wing structure at 300 kN.

literature, and Cardiff University has not performed a material characterisation test campaign before the experimental test. Because of the manufacturing process, the material properties are expected to vary in their nominal values. Cardiff University will perform a material characterisation a posteriori.

The modelling of the bolts gives another reason for the differences.

Due to numerous bolts adopted in the structure and the high modelling times required to model each joint, the partners have modelled the connections between the different components of the representative wing structure as bonded surfaces, while POLITO modelled bolts and contact between components. The assumption of considering bonding surfaces as representative connections between components, greatly
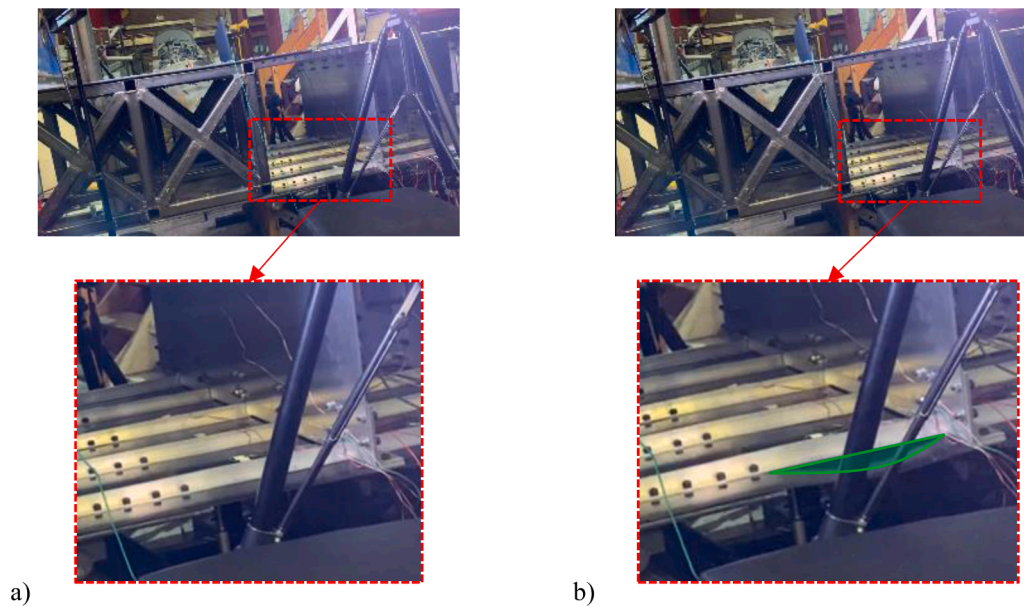
Fig. 19. Experimental images: (a) at the beginning of the test;
(b) at maximum load, 300 kN (the green-shaded area shows the buckling of the lower skin panel).

simplifying the numerical models in terms of computational time. However, the displacements and the deformations resulting from the numerical analysis can differ from those obtained experimentally due to neglecting any sliding between contacting surfaces.

One of the main reasons of the differences between the stiffness predicted by the numerical models and the experiment is the modelling of the boundary conditions. The loading supports of the wing structure consist of cylinders, as presented in Fig. 5. The different partners modelled these boundary conditions differently. Some partners have modelled the cylindrical supports (KTU, BELGRADE), while others have replaced the cylinders enforcing specific boundary conditions for the displacement's degree of freedom on the nodes in contact between the representative wing structure and the loading support. However, supports were mounted on a truss structure during the experimental test, increasing the total compliance of the tested structure.

The presence of initial imperfections can also explain some differences. The initial curvature in the experimental load vs displacement data given in Fig. 14 shows initial imperfections/gaps between the loading structures and the tested structure, which has not been considered in any numerical models.

The experimental failure mode observed is due to the debonding between multiple stiffeners and the composite plate. This initial debonding is a local failure mode, mostly dictated by the applied displacement that induces shear sliding in this critical region due to the bending mismatch between the stiffeners and the plate.

6. Conclusions

This paper presents a preliminary benchmark to predict the response of a wing structure subjected to 4-point loading through different FE modelling efforts.

Six partners of the COST project ODIN independently developed the FE models, based on their backgrounds in numerical analyses, to predict the structural behaviour, receiving only the drawing of the structure, the material properties, the loading and boundary conditions. The different partners conducted quasi-static and dynamic analyses using different element types (shell, solid, beam).

The experimental results showed a linear load-displacement characteristics and this behaviour was captured by the numerical models at various extent. The experiment setup resulted in less stiffness when compared to the numerical models, which might be due to several reasons, including possible clearances between the mounted parts, excessive compliance of the supporting structure and inaccurate material property data. Despite these differences, the predicted initial stiffness was consistent amongst the different numerical models, and some analyses could capture the ultimate displacement with a good approximation.

The preliminary study presented in this paper highlights the importance of a detailed modelling of the entire experimental apparatus, including boundary conditions, initial imperfections and instrumentation position. It reveals the limitations of some simplifying assumptions usually made in the numerical models when predicting the behaviour of large and complex structures.

The structural details that are fundamental to accurate predictions will be included in future numerical analyses conducted by the partners as part of the second phase of the COST project ODIN. In addition, another test will be conducted at Cardiff University with more detailed measurements of the structure and the rig fixture.

Declaration of Competing Interest

The authors declare that they have no known competing financial interests or personal relationships that could have appeared to influence the work reported in this paper.

References

[1] P. Davies, D.R. Moore, Glass/nylon-6.6 composites: delamination resistance testing, Compos. Sci. Technol. 38 (3) (1990) 211–227, https://doi.org/10.1016/0266-3538(90)90059-E.

[2] P. Davies, C. Moulin, H.H. Kausch, M. Fischer, Measurement of GIc and GIIc in carbon/epoxy composites, Compos. Sci. Technol. 39 (3) (1990) 193–205, https://doi.org/10.1016/0266-3538(90)90041-3.

[3] P. Davies, H.H. Kausch, J.G. Williams, A.J. Kinloch, M.N. Charalambides, A. Pavan, D.R. Moore, R. Prediger, I. Robinson, N. Burgoyne, K. Friedrich, H. Wittich, C. A. Rebelo, A. Torres Marques, F. Ramsteiner, B. Melve, M. Fischer, N. Roux, D. Martin, P. Czarnocki, D. Neville, I. Verpoest, B. Goffaux, R. Lee, K. Walls, N. Trigwell, I.K. Partridge, J. Jaussaud, S. Andersen, Y. Giraud, G. Hale, G. McGrath, Round-robin interlaminar fracture testing of carbon-fibre-reinforced epoxy and PEEK composites, Compos. Sci. Technol. 43 (2) (1992) 129–136, https://doi.org/10.1016/0266-3538(92)90003-L.

[4] M.J. Hinton, P.D. Soden, Predicting failure in composite laminates: the background to the exercise, Compos. Sci. Technol. 58 (7) (1998) 1001–1010, https://doi.org/10.1016/S0266-3538(98)00074-8.

[5] P.D. Soden, M.J. Hinton, A.S. Kaddour, A comparison of the predictive capabilities of current failure theories for composite laminates, Compos. Sci. Technol. 58 (7) (1998) 1225–1254, https://doi.org/10.1016/S0266-3538(98)00077-3.

[6] S.B. Clay, S.P. Engelstad, Benchmarking of composite progressive damage analysis methods: the background, J. Compos. Mater. 51 (10) (2017) 1325–1331, https://doi.org/10.1177/0021998316672520.

[7] S.P. Engelstad, S.B. Clay, Comparison of composite damage growth tools for fatigue behavior of notched composite laminates, J. Compos. Mater. 51 (15) (2017) 2227–2249, https://doi.org/10.1177/0021998317694948.

[8] T. Bach, S. Dähne, L. Heinrich, C. Hühne, Structural optimization of composite wings in an automated multi-disciplinary environment, in: Proceedings of the 14th AIAA Aviation Technology, Integration, and Operations Conference, 2014, p. 2295, https://doi.org/10.2514/6.2014-2295.

[9] W. Yang, Z. Yue, L. Li, P. Wang, Aircraft wing structural design optimization based on automated finite element modelling and ground structure approach, Eng. Optim. 48 (1) (2016) 94–114, https://doi.org/10.1080/0305215X.2014.995175.

[10] O. Stodieck, J.E. Cooper, P.M. Weaver, Aeroelastic tailoring of a representative wing box using tow-steered composites, AIAA J. 54 (2017), https://doi.org/10.2514/1.J055364.

[11] Y. Wang, X. Ouyang, H. Yin, X. Yu, Structural-optimization strategy for composite wing based on equivalent finite element model, J. Aircr. 53 (2) (2016) 351–359, https://doi.org/10.2514/1.C033469.

[12] J.G. Bakuckas, C. Reewanshu, P. Swindell, M. Fleming, J.Z. Lin, J.B. Ihn, N. Desai, E. Espinar-Mick, M. Freisthler, Bonded repairs of composite panels representative of wing structure. ICAF 2019-Structural Integrity in the Age of Additive Manufacturing, 2019, https://doi.org/10.1007/978-3-030-21503-3_45.

[13] R.B. Kumar, Investigation on buckling response of the aircraft's wing using finite-element method, Aust. J. Mech. Eng. 18 (2020) 122–131, https://doi.org/10.1080/14484846.2018.1483467.

[14] Z. Kapidžić, L. Nilsson, H. Ansell, Finite element modeling of mechanically fastened composite-aluminum joints in aircraft structures, Compos. Struct. 109 (2014) 198–210, https://doi.org/10.1016/j.compstruct.2013.10.056.

[15] COST Action CA 18203, Optimised design for inspection, http://odin-cost.com/, 2022 (accessed 10 April 2022).

[16] European Cooperation in Science and Technology (COST), https://www.cost.eu/, 2022 (accessed 10 April 2022).

[17] A. Raimondo, C. Bisagni, Fatigue analysis of a post-buckled composite single-stringer specimen taking into account the local stress ratio, Compos. Part B Eng. 193 (2020), https://doi.org/10.1016/j.compositesb.2020.108000.

[18] A. Raimondo, I. Urcelay Oca, C. Bisagni, Influence of interface ply orientation on delamination growth in composite laminates, J. Compos. Mater. (2021), https://doi.org/10.1177/00219983211031636.

[19] M.F.S.F. de Moura, J.P.M. Gonçalves, F.G.A. Silva, A new energy based mixed-mode cohesive zone model, Int. J. Solids Struct. 102-103 (2016) 112–119, https://doi.org/10.1016/j.ijsolstr.2016.10.012.

[20] M.F.S.F. de Moura, J.P.M. Gonçalves, Cohesive zone model for high-cycle fatigue of composite bonded joints under mixed-mode I+II loading, Eng. Fract. Mech. 140 (2015) 31–42, https://doi.org/10.1016/j.engfracmech.2015.03.044.

[21] H. Gedikli, Ö.N. Cora, M. Koç, Comparative investigations on numerical modeling for warm hydroforming of AA5754-O aluminum sheet alloy, Mater. Des. 32 (5) (2011) 2650–2662, https://doi.org/10.1016/j.matdes.2011.01.025.

[22] F. Güner, H. Sofuoglu, Ö.N. Cora, An investigation of contact interactions in powder compaction process through variable friction models, Tribol. Int. 96 (2016) 1–10, https://doi.org/10.1016/j.triboint.2015.12.016.

[23] S. Patil, I. Atanasovska, S. Karuppanan, Contact stress evaluation of involute gear pairs, including the effects of friction and helix angle, J. Tribol. T. ASME 137 (4) (2015), 044501, https://doi.org/10.1115/1.4030242.

[24] I. Atanasovska. The influence of load and boundary conditionsimulation on the structural evaluation of railway wagons with finite element tools, Third Serbian Congress on Theoretical and Applied Mechanics, Vlasina lake, Serbia, 5-8 July 2011, Section C – Mechanics of solid bodies, Publisher: Serbian Society of Mechanics, Serbia, 2011, pp. 352–365. ISBN 978-86-909973-3-6.

[25] G. Frulla, Structural behavior of damaged anisotropic stiffened panels undercompressive loads, in: Proceedings of the 25th Congress of International Council of the Aeronautical Science, 25th ICAS Conference 3-8 September 2006, Hammburg, Germany. ISBN 0-9533991-7-6. CD Published by Optimage Ltd. on behalf of the International Council of the Aeronautical Sciences (ICAS).

[26] A. Polla, P. Piana, E. Cestino, G. Frulla, Delamination and fracture modeling techniques for shell composite structures in LS-DYNA®, in: Proceedings of the 13th European LS-DYNA Conference 4-7, Ulm Germany, 2021. October.

[27] R. Troian, L. Khalij, D. Lemosse, E. Souza, Uncertainty analysis of structural response under a random impact, Optim. Eng. 22 (2021) 2429–2456, https://doi.org/10.1007/s11081-021-09679-z.

[28] R. Troian, K. Shimoyama, F. Gillot, S. Besset, Methodology for the design of the geometry of a cavity and its absorption coefficients as random design variables under vibroacoustic criteria, J. Comput. Acoust. 24 (02) (2016), 1650006, https://doi.org/10.1142/S0218396×16500065.

[29] D. Systèmes, Abaqus® 2019 Documentation, Simulia Corp, Providence, RI, USA, 2019.

[30] D. Simulia, ABAQUS 6.11 analysis user's manual, 2011.

[31] ANSYS 2020 Documentation, R2, ANSYS Inc., 2020.

[32] Academic Research Mechanical, Release 19.3, Help System, Mechanical APDL Structural Analysis Guide, ANSYS, Inc, USA.

[33] Livermore Software Technology Corporation, LS-DYNA Keyword User's Manual - Volume 1, LS-DYNA R11.1,2018.

[34] Livermore Software Technology Corporation, LS-DYNA Keyword User's Manual - Volume 1, LS-DYNA R9.1.0,2017.